mathematics

MDPI

Article

Numerical Study of the Thermal Energy Storage Container Shape Impact on the NePCM Melting Process

Obai Younis [1,*], Naef A. A. Qasem [2], Aissa Abderrahmane [3] and Abdeldjalil Belazreg [3]

[1] Department of Mechanical Engineering, College of Engineering in Wadi Alddawasir, Prince Sattam Bin Abdulaziz University, Al Kharj 11942, Saudi Arabia
[2] Department of Aerospace Engineering and Interdisciplinary Research Center for Aviation and Space Exploration, King Fahd University of Petroleum and Minerals (KFUPM), Dhahran 31261, Saudi Arabia; naefqasem@kfupm.edu.sa
[3] Laboratory of Quantum Physics of Matter and Modeling Mathematics (LPQ3M), University of Mustapha Stambouli of Mascara, Mascara 29000, Algeria; a.aissa@univ-mascara.dz (A.A.); abdeldjalil.belazreg@univ-mascara.dz (A.B.)
* Correspondence: o.elamin@psau.edu.sa

Abstract: Recently, thermal energy storage has emerged as one of the alternative solutions to increase energy efficiency. The geometry of a thermal energy storage container holds a significant role in increasing the heat transmission rates in the container. In this article, we examined the influence of the inner and outer tube shapes of a shell and tube LHTES on the thermal activity within the system. The gap between the inner and outer tube is loaded with nano-enhanced phase change material (NePCM); hot fluid is passed through the inner tube while the outer tube is insulated. COMSOL commercial software (version 6.2) was used to numerically simulate the NePCM melting process. Mainly, six different geometries were investigated with inner or outer tubes with trefoil, cinquefoil, and heptafoil shapes. The influences of nanoparticles volumetric fraction (ϕ = 0–8%) were also discussed. The findings are displayed and discussed in terms of the average Nusselt number, the average liquid fraction, the total energy generation, and the average temperature. The findings showed that the melting process is highly affected by the shape of the inner tube and ϕ, while the outer tube shape impact is less important. It was noticed that employing an inner tube with a trefoil improved the melting process by more than 25% while increasing the ϕ from 0 to 8% resulted in reducing the melting time by up to 20%.

Keywords: LHTES; NePCM; container shape; melting process

MSC: 35Q30; 80A19; 80A22

Citation: Younis, O.; Qasem, N.A.A.; Abderrahmane, A.; Belazreg, A. Numerical Study of the Thermal Energy Storage Container Shape Impact on the NePCM Melting Process. *Mathematics* **2024**, *12*, 3954. https://doi.org/10.3390/math12243954

Academic Editors: Zacharias Anastassi, Athinoula A. Kosti and Mufutau Ajani Rufai

Received: 13 November 2024
Revised: 9 December 2024
Accepted: 11 December 2024
Published: 16 December 2024

1. Introduction

There has been a notable shift over the past few years in the worldwide energy situation, primarily prompted by the growing need for eco-friendly and sustainable energy alternatives. The shift towards renewable energy generation, namely solar and wind power, has resulted in an increasing emphasis on the advancement of energy storage systems capable of efficiently handling the sporadic nature of these sources. Phase change materials (PCMs) are used in several areas, such as thermal energy storage, waste heat preservation, and solar power utilization [1–3]. The technology has the capacity to store and release Significant quantities of energy at a moderate expense and with exceptional effectiveness.

PCMs, on the other hand, don't conduct heat well, so the thermal performance of LHTES systems is limited [4,5]. Hence, it is imperative to implement steps to enhance the heat transfer mechanism between the fluid and PCM. Various techniques to enhance

the PCM thermal conductivity are utilized, such as introducing fins [6–9], dispersing nanoparticles [10–12], and inserting porous media [13–15].

Among the abovementioned approaches that improve thermal conductivity, the container of LHTES not only keeps the PCM in place but also changes the flow of heat inside the storage, which in turn changes how well it works [15–17]. We commonly use rectangular [18,19], cylindrical [20,21], and sphere [22–24].

Zhen Qin et al. [25] examined the melting characteristics of PCM within a LHTES. The results indicated that the shape of the container has an impact on the way the PCM melts by altering the free convection. The alteration in container shape has a beneficial effect on the surface contact area for both the fluid and the PCM, hence improving its rates of charging and discharging.

In their study, Bingkun Huang et al. [26] improved the container design to address the issue of very slow melting rates for the residual PCM in the bottom of the container. The authors suggested novel PCM container designs to improve the rate of melting by strengthening the convection current.

In a TTHX, Boujelbene et al. [27] investigated the charging process inside a zigzag-shaped middle tube design. They reported that the zigzag-shaped tube design reduced the melting time by 82%.

Li et al. [28] did a study on how various tube shapes in a star-shaped shell affect the solidification of NE PCM. They found that increasing the amplitude of the star profile resulted in reducing the time needed for complete solidification.

Najafpour and Abidi [29] performed computational modeling to improve the thermal efficiency of LHTES systems by using perforated stair fins and altering the design of the enclosure. Parametric tests were performed to evaluate the influence of fin perforations with varied sizes and variable amounts of holes. They determined that they noted substantial improvements in the mean Nusselt numbers for parallelogram, trapezoidal, and rectangular containers, with corresponding increases of 95%, 114%, and 133%. Consequently, the enhancement in heat transmission has resulted in a reduction in the duration it takes for the materials to melt by 44.5 min, 47.5 min, and 51.5 min, respectively.

Nematpour Keshteli et al. [30] researched the influence of a lobed inner tube design on the melting performance of phase change material in a double-pipe energy storage system. The research performed melting studies on metal foam, nanoparticles, and PCM composition using different lobe geometry.

Rehan Qaiser et al. [31] investigated the impact of tubes and shell shapes on the LTES system's thermal performance enhancement. They investigated tube geometries of hexagonal, pentagonal, square, and triangular shapes. The study by Khedher et al. [32] tried to improve the melting performance of a vertical latent heat two-tube heat exchanger by changing the design of the container that held the PCM. This investigation illustrates the inherent capacity for geometric modifications to improve thermal energy storage capacity. Rabienataj et al. did research [33]. The study demonstrated the melting behavior of a specific PCM called N-eicosane. The PCM was held in a cylindrical annulus LHTES system that was positioned horizontally. In their investigation, they analyzed the combined impact of radial fins, nanoparticles, and geometry adjustment to identify the most effective arrangement. In order to determine the optimal aspect ratio and orientation of the ellipse, they used three distinct annulus configurations: two circular cylinders, one elliptical cylinder inside a circular cylinder, and one cylinder with fins. According to their findings, altering the shape might enhance the free convection phenomenon occurring at the lower part of the annulus, which exhibited a slow rate of melting.

The incorporation of nanoparticles into liquids and materials has garnered significant interest across several disciplines, owing to the distinctive characteristics and possible advantages that nanoparticles possess [34,35]. Nanoparticles are tiny particles that have diameters on the nanometer scale, often ranging from 1 to 100 nm. They may be fabricated using a diverse array of materials, including metals, metal oxides, polymers, and others, each with distinct features [36,37]. Faraji et al. [38] examined the kinetics of solid-liquid

phase transition in n-eicosane with the addition of nanoparticles. The study was conducted in an enclosure specifically constructed for cooling electronic devices. The research analyzed situations involving one, two, and three electrical components that were sticking out. Their research showed that the inclusion of SiO2-MWCNT hybrid nanoparticles significantly extended the time it took for the material to melt, with an increase of roughly 92% in comparison to the pure PCM sample. Hasnain et al. [39] improved the melting process of PCM by incorporating branching fins and nanoparticles in a horizontal orientation. The findings indicate that including nanoparticles in the PCM at volumes of 1%, 5%, and 10% reduced the total melting time by 11.5%, 19.2%, and 26.8%, respectively. Al-Jethelah et al. [40] investigated the phase transition of a NePCM in a square container with a heated left wall and a permeable metal. They discovered that the rate of melting increases when the Rayleigh and Darcy numbers are larger. Ebrahimi and Dadvand [41] also investigated a square cavity loaded with a nanofluid containing PCM, where two pairs of heat sources were present. The researchers determined that a 2% volume concentration of the nanoparticles resulted in the most rapid melting rate, regardless of the heat source locations being investigated.

In their investigation, Vednath et al. [42] assessed the effectiveness of a hybrid nanomaterial consisting of CuO and MWCNT on paraffin wax. The findings revealed a 6.1% enhancement in heat conductivity for the NePCM in comparison to pure paraffin wax. Additionally, there was a significant 66.6% decrease in the time needed for the solid-to-liquid phase transition. In a comparable investigation, Sheikholeslami and Khalili [43] studied the effects of using nanoparticles to cool solar panels when a Fresnel lens is present. Their research included the use of nanomaterials in the two parts of the filtration and conditioning duct, uncovering encouraging outcomes.

Previous research on the charging process has emphasized the need to minimize the time of the process as a critical goal for any system. As a result, scientists have investigated many methods, and the use of nanoparticles has emerged as a particularly successful way. In this investigation, the previously described approach was utilized to improve the charging rates. The Cu nano-additives possess either inner or exterior tubes with trefoil (three waves), cinquefoil (five waves), or heptafoil (seven waves) shapes. The FEM was utilized to resolve the governing equations. The constantly evolving character of this occurrence was carefully recorded and displayed in various arrangements. In addition, the required time periods for each individual step were carefully recorded.

2. Problem Description

The research utilizes undulating walls to accelerate the charging process of a shell-and-tube latent heat thermal energy storage (LHTES) unit. Figure 1 displays the cross-section that has been studied, together with its boundary conditions. The container is loaded with a composite material consisting of paraffin wax reinforced with nanoparticles of copper (Cu). The copper nanoparticles have a diameter of 50 nm and volumetric fractions of 0% (pure PCM), 4%, and 8%. The heating liquid flows in the inner tube while the external tube is insulated.

The functions of the wavy cylinder surface are [44]

$$r_1(\eta) = (r + A\cos(2\pi N\eta)) \times \sin(2\pi\eta) \quad (1)$$

$$r_2(\eta) = (r + A\cos(2\pi N\eta)) \times \cos(2\pi\eta). \quad (2)$$

Here, r denotes the radius of the smooth (base) circle, η denotes the angular coordinate, A and N are the amplitude of the wavy cylinder's wave and the number of waves. The properties of the material used are listed in Table 1.

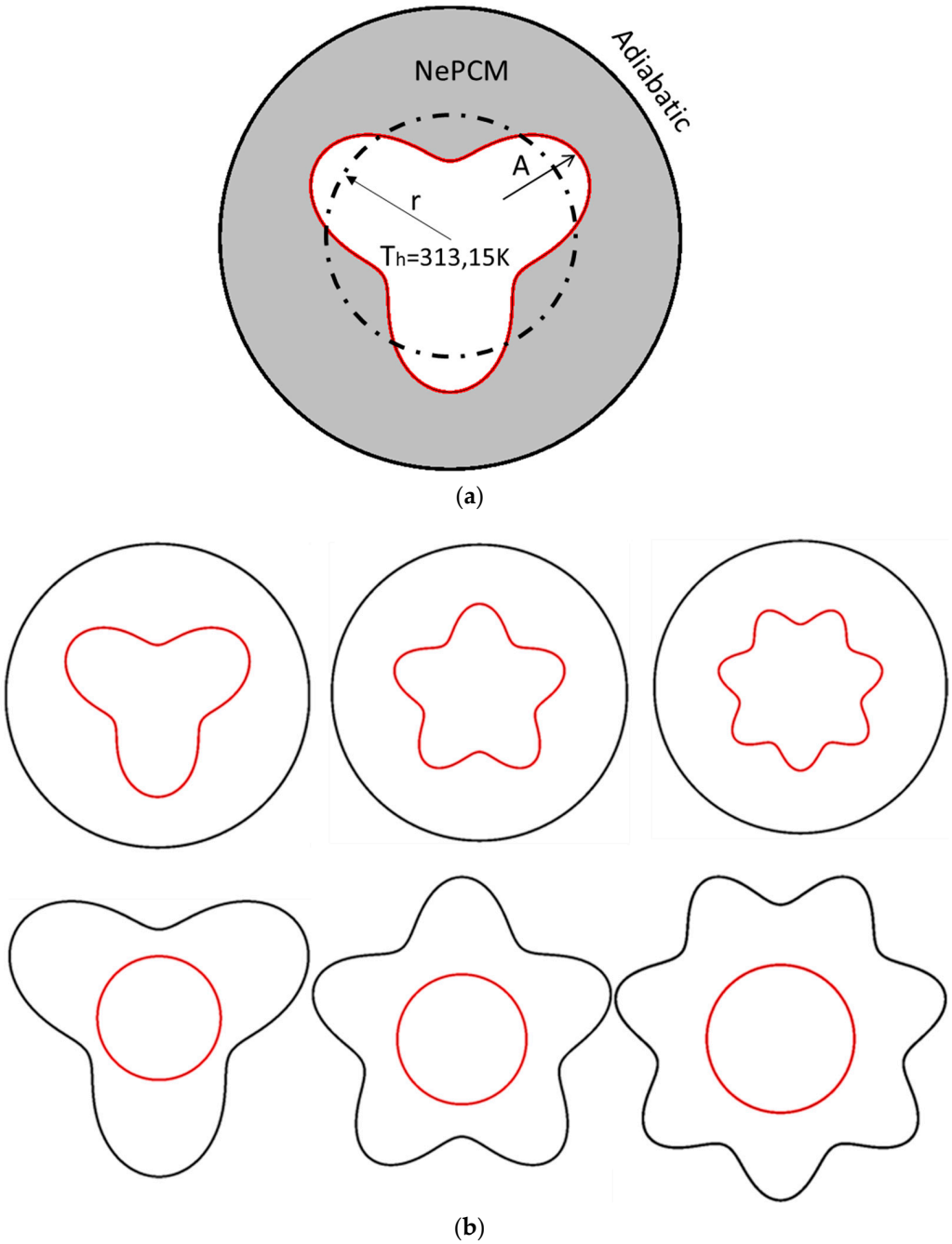

Figure 1. (**a**) boundary condition, (**b**) Case studies of different geometries (inner or outer tube with trefoil, cinquefoil, and heptafoil shapes).

Table 1. Thermophysical characteristics of the materials [45].

Melting temperature	28–30 °C
Density (solid-liquid)	870–760 kg/m^3
Kinematics Viscosity	3.42×10^{-3} m^2/s
Specific Heat (solid-liquid)	2400–1800 J/kgK
Thermal Conductivity (solid-liquid)	0.24–0.15 W/mK
Latent Heat of Fusion	179 kJ/kg
Thermal Expansion Coefficient	0.0005 K^{-1}

3. Numerical Model

3.1. Assumptions and Governing Equations

In order to simplify the numerical model, the following assumptions were put forward:

- The liquid PCM exhibits properties of homogeneity, incompressibility, and Newtonian fluid behavior when flowing under laminar conditions. Moreover, the solid phase change material (PCM) demonstrates a condition characterized by a homogeneous composition and uniformity [46].
- The change in volume that occurs during the change from the fluid phase to the solid phase is negligible.
- The 2D free convection takes place within the liquid phase.
- The density variation is modeled by the Boussinesq approximation.

Given the assumptions provided, it is feasible to deduce the governing equation for the NePCM melting process as follows: Continuity equation:

$$\nabla \cdot \vec{V} = 0 \tag{3}$$

Momentum equation:

$$\frac{\partial \vec{V}}{\partial t} + \vec{V} \cdot \nabla \vec{V} = \frac{1}{\rho}\left(-\nabla P + \mu \nabla^2 \vec{V} + \rho \beta \vec{g}(T - T_{\text{ref}})\right) + \vec{S} \tag{4}$$

Energy equation:

$$\frac{\partial h_{\text{sens}}}{\partial t} + \frac{\partial h_{\text{lat}}}{\partial t} + \nabla \cdot \left(\vec{\nabla} h_{\text{sens}}\right) = \nabla \cdot \left(\frac{k}{\rho c_\rho} \nabla h_{\text{sens}}\right) \tag{5}$$

where h_{sens} is the sensible enthalpy, which is given by:

$$h_{\text{sens}} = h_{\text{ref}} + \int_{T_{\text{ref}}}^{T} c_P \, \mathrm{d}T = h_{\text{ref}} + c_P \int_{T_{\text{ped}}}^{T} \mathrm{d}T \tag{6}$$

The latent enthalpy h_{lat} reads:

$$h_{\text{lat}} = \lambda L \tag{7}$$

where L is the latent heat of the material, and λ can be defined as: [47]

$$\lambda = \begin{cases} \frac{h_{\text{lat}}}{L} = 0 & \text{if } T < T_{\text{s}} \\ \frac{h_{\text{lat}}}{L} = 1 & \text{if } T > T_{\text{liq}} \\ \frac{h_{\text{lat}}}{L} = \frac{T - T_{\text{s}}}{T_{\text{liq}} - T_{\text{s}}} & \text{if } T_{\text{s}} < T < T_{\text{liq}} \end{cases} \tag{8}$$

The NePCM density reads [48,49]:

$$\rho_{n\bar{p}} = (1 - \varphi)\rho_p + \varphi \rho_n \tag{9}$$

The NEPCM heat capacity term reads:

$$(\rho C_p)_{np} = (1 - \varphi)(\rho C_p)_p + \varphi (\rho C_p)_n \tag{10}$$

The Boussinesq term reads:

$$(\rho \beta)_{n\rho} = (1 - \varphi)(\rho \beta)_p + \varphi (\rho \beta)_n \tag{11}$$

The volumetric proportion of nanoparticles is represented by the symbol φ, with subscripts np, s, and p denoting NePCM, solid particle, and PCM, respectively. The Brinkman equation mathematically represents the effective dynamic viscosity of the NePCM [50]:

$$\mu_{np} = \frac{\mu_p}{(1-\varphi)^{2.5}} \tag{12}$$

The thermal conductivity of the immobile NePCM, represented as subscript 0, is defined by Maxwell's equation [51]:

$$\frac{k_0}{k_p} = \frac{k_n + 2k_p - 2\varphi(k_p - k_n)}{k_n + 2k_p + \varphi(k_p - k_n)} \tag{13}$$

NEPCM's effective thermal conductivity reads:

$$k_{np} = k_0 + k_d \tag{14}$$

where k_d is the thermal conductivity improvement term, it reads:

$$k_d = C(\rho c_p)_\varphi \left|\vec{V}\right| \varnothing d_u \tag{15}$$

The value of C is determined based on the investigation done by Wakao and Kaguei [52]. The expression for the latent heat of the NePCM is given by [53]:

$$(\rho L)_{np} = (1-\varnothing)(\rho L)_p \tag{16}$$

In order to account for the influence of phase shift on convective heat transfer, a damping factor designated as $\vec{S}$ and derived from Darcy's law, is incorporated into the momentum equation as a source component, referred to as Equation (2). The precise meaning of this source phrase is given below [54]:

$$\vec{S} = \frac{(1-\lambda)^2}{\lambda^3 + 0.001} A_{mush} \vec{V} \tag{17}$$

In the present investigation, the constant parameter A_{mush} is commonly given a value of 10^6. The mushy zone constant is a significantly large numerical number, often ranging from 10^4 to 10^7 [55,56]. The value of χ is a tiny integer used to avoid division by zero.

The entropy created owing to flow irreversibility caused by the friction factor is expressed as:

$$S_f = \frac{\mu_{np}}{\overline{T}} \left\{ 2\left[\left(\frac{\partial \overline{u}}{\partial x}\right)^2 + \left(\frac{\partial \overline{v}}{\partial y}\right)^2 \right] + \left(\frac{\partial \overline{u}}{\partial x} + \frac{\partial \overline{v}}{\partial y}\right)^2 \right\} \tag{18}$$

The produced entropy due to the heat transmission reads;

$$S_{ht} = \frac{k_{np}}{\overline{T}^2} \left[\left(\frac{\partial \overline{T}}{\partial x}\right)^2 + \left(\frac{\partial \overline{T}}{\partial y}\right)^2 \right] \tag{19}$$

$$S_{tot} = S_{ht} + S_f \tag{20}$$

3.2. Boundary and Initial Conditions

The initial temperature of the PCM T_0 was set to 24 °C, and T_H = 40 °C. The external surface of the shell is thermally insulated.

Figure 2 presents the flowchart illustrating the computational method used in the present investigation.

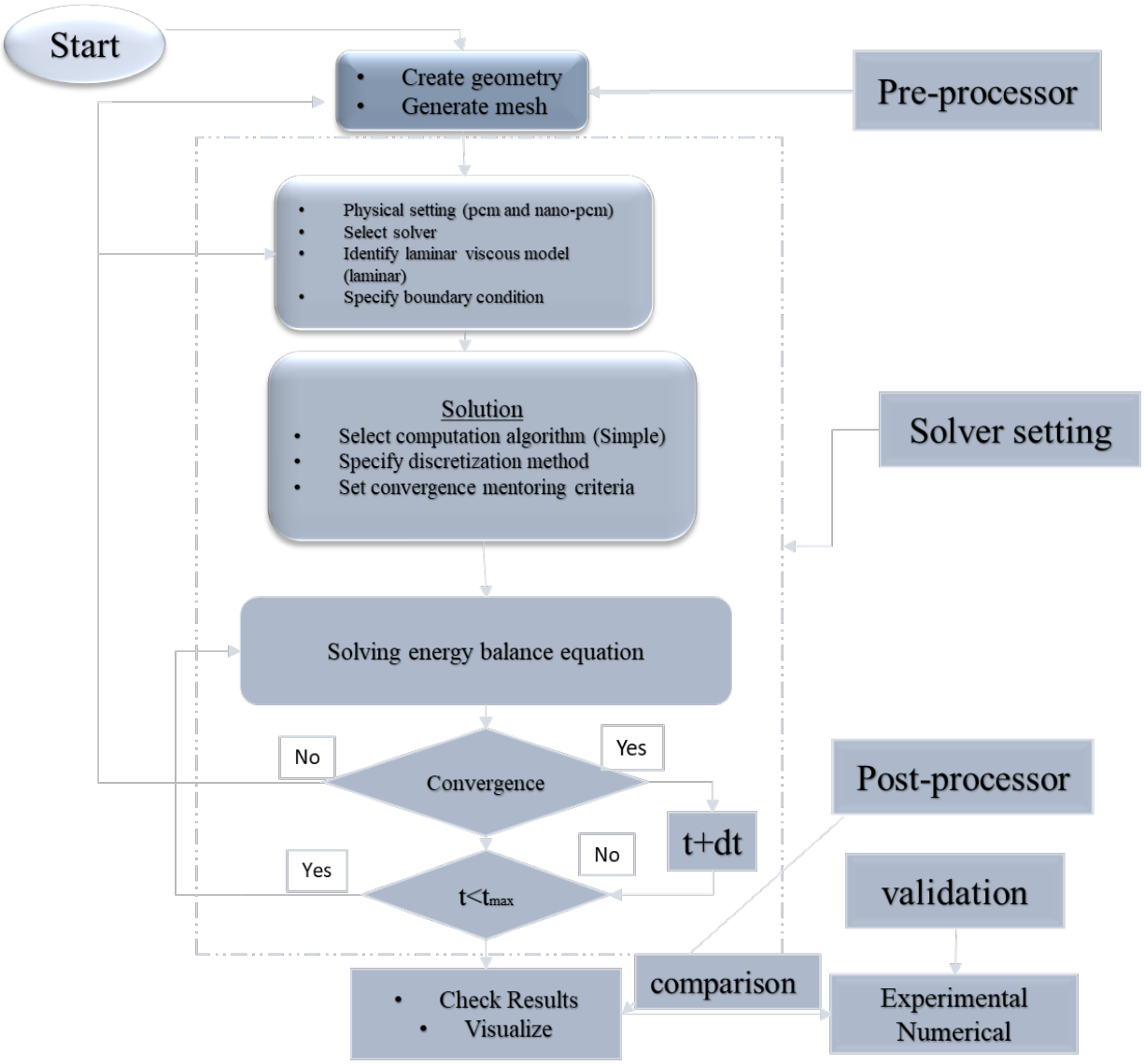

Figure 2. The flowchart for numerical calculation.

3.3. Grid and Validation Study

Figure 3a illustrates the average liquid flow as a function of time for a variety of cell numbers. The different studied grids are given in Table 2. In this investigation, we have selected S2 with 18,263 elements, which is an extra-fine optimum size that requires less time than S3 for no discernible reason.

Computational methods are employed in the subsequent phase to ascertain the results. A Galerkin Finite Element method is employed to address the previously mentioned PDEs (3)–(5), encompassing the flow and heat transfer processes along with the additional boundary conditions. The weak forms of the governing equations are established, and a non-uniform mesh separation is implemented. Figure 3b presents a comprehensive account of the process, illustrating the validation of the algorithm through Darzi's [45] numerical model. This model employs RT27 as a phase change material, with its physical properties outlined in Table 1. We compare the solution for phase charging distribution in a square cavity with the computational results presented by Darzi et al. [45]. Figure 3b demonstrates this contrast. The observed findings align closely with previously published material, thereby confirming the fundamental validity of the computational model.

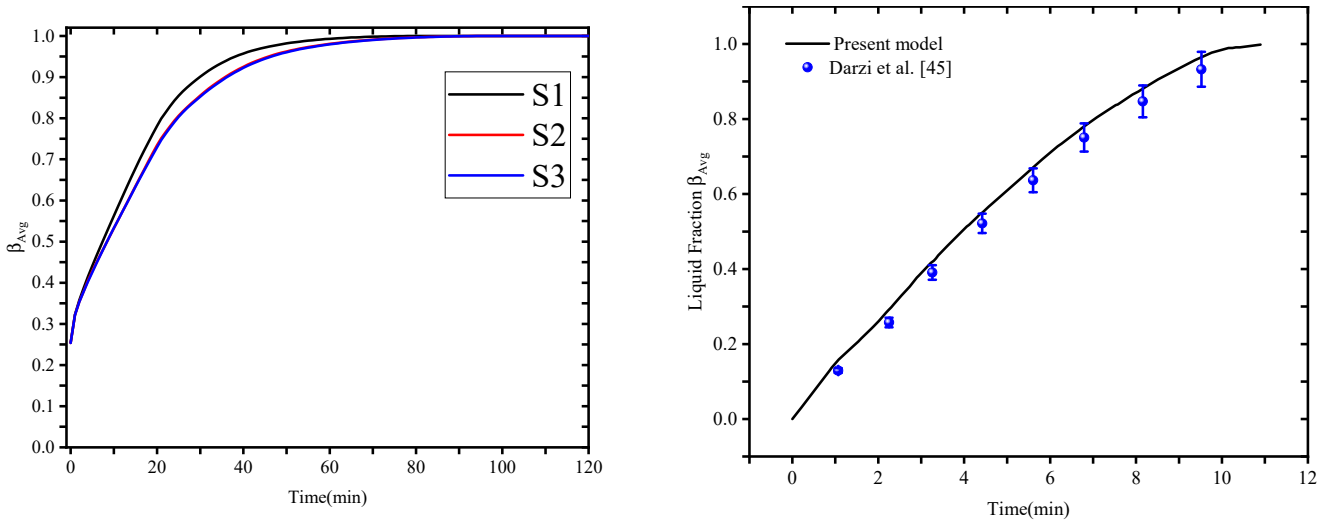

(**a**) (**b**)

Figure 3. (**a**) Evolution of liquid fraction with three schemes of mesh elements, and (**b**) validation against the reported results of Darzi. A. (2015).

Table 2. Mesh independence study.

Grid	S1	S2	S3
Element size	6378	18,263	20,796

4. Results and Discussion

The different geometries shown in Figure 1 are analyzed for the NEPCM melting process. The geometries have either inner or external tubes with trefoil (three waves), cinquefoil (five waves), or heptafoil (seven waves) shapes. The annular region is filled with copper nanoparticle-enhanced n-octadecane paraffin PCM. The heating liquid flows in the inner tube while the external tube is insulated. The results are represented by temperature, liquid fraction, and liquid phase speed contours, as well as temporal profiles of average temperature, average liquid fraction, average Nusselt number, and average entropy (total: thermal and flow friction). The impact of the inner tube's shape, the external tube's shape, and the concentration of nanoparticles are discussed in detail.

4.1. Impact of the Inner Tube Shape

The effect of the inner tube shape is investigated in terms of the number of waves (N), which is 3 for trefoil, 5 for cinquefoil, and 7 for heptafoil. Figure 4 shows the temperature, melting process, and liquid phase speed contours at a melting time of 25 min. The higher temperature values exist at the top of the thermal storage unit, affected by the buoyancy effect of the melted PCM. The process starts with a conduction heat transfer from the inner tube wall to the neighbor PCM until the melting process starts. After that, the convection heat transfer occurs in the melted region as the hot regions experience low-dense PCM, rising up. This is the explanation of why the top regions are hot. The bottom regions are still at low temperatures due to the low amount of heat transfer by conduction, while convection has not reached this region yet after 25 min.

Analyzing the temperature and liquid fraction contours provides a comprehensive understanding of how varying the number of waves (N = 3, 5, and 7) influences heat transfer and the melting process, particularly in the lower region of the system. At the specific time investigated (25 min), it is observed that heat transfer to the lower segment predominantly occurs through conduction. This is primarily due to the minimal influence of convective effects in this region, which is characteristic of the conditions examined. The conduction process is marked by a radial outward propagation of heat from the inner

tube, accompanied by a gradual downward movement that reflects the thermal gradient established by the heating fluid.

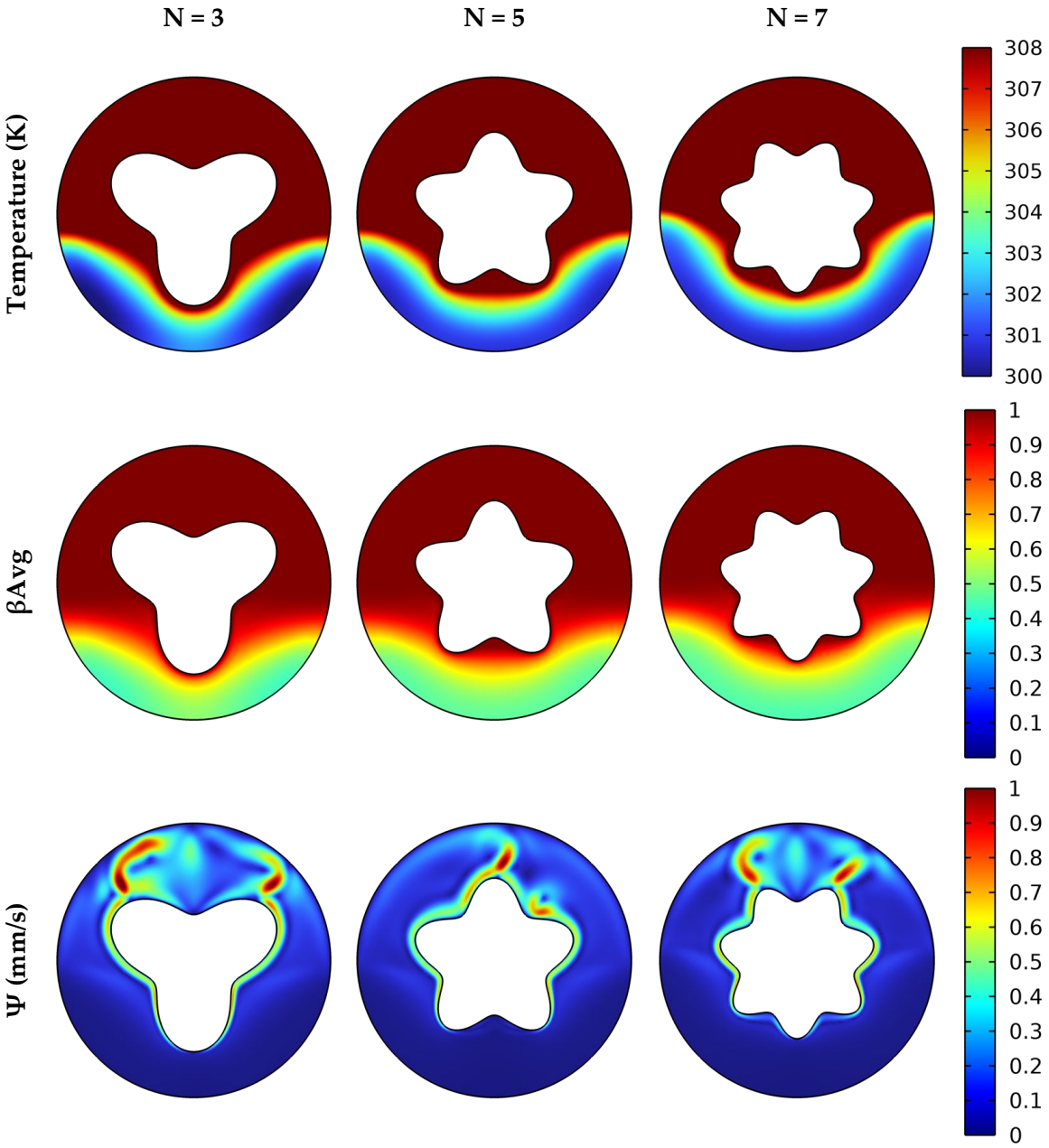

Figure 4. Effect of inner tube wave number on temperature, average liquid fraction, and velocity in t = 25 min.

The design of the inner tube is pivotal in reducing thermal resistance. By minimizing the distance between the inner and outer tubes, this configuration enables more effective heat transfer, thus accelerating the melting of the phase change material (PCM).

In the case of the N = 3 configuration, the longer, curved surface of the trefoil geometry provides a more extensive contact area that effectively reaches into the bottom region. This results in a heightened conduction effect, allowing for more efficient heat delivery, which significantly enhances the melting process in that area. In contrast, the configurations with N = 5 and N = 7 introduce a greater number of waves, which shortens the wavelengths to maintain adequate flow area for the heating fluid. Although this design feature is beneficial for maintaining fluid dynamics, it inadvertently increases the distance between the PCM

and the heat source. This extended distance diminishes the efficiency of heat transfer through conduction, ultimately prolonging the melting process in these configurations.

Additionally, the buoyancy effect plays a crucial role in the melting dynamics observed within the system. In regions adjacent to the inner tube, where temperatures are elevated, buoyancy causes the establishment of natural convection currents. This phenomenon facilitates the upward and outward propagation of heat, effectively distributing thermal energy more uniformly. The velocity contours measured in these regions exhibit significantly higher values, particularly near the inner tube's corners, where the interplay between heat and fluid dynamics is most pronounced.

In the N = 3 configuration, enhanced velocities are detected at the top left and right regions, promoting improved circulation of the fluid flow. This increased flow velocity contributes to a more effective distribution of heat, which synergistically improves the melting process. The enhanced convective heat transfer here acts as a complement to the conduction-driven heat transfer taking place at the bottom, rendering the N = 3 configuration particularly efficient.

Moreover, the strategic downward positioning of a wave in the N = 3 design directly targets the lower region, optimizing both conduction and buoyancy-enhanced heat transfer mechanisms. This deliberate design choice positions the N = 3 configuration as the most effective in achieving efficient melting, integrating the benefits of both heat transfer modes to maximize the overall melting efficiency.

As Figure 4 shows the results qualitatively, the proper comparison between the three cases can quantitatively be evaluated by temporal curves for the results, as exhibited in Figure 5. It is shown that keeping heating the NEPCM results in an increase of average temperature and liquid fraction of the PCM until reach equilibrium values. For N = 3, the maximum temperature (312 K) and complete melting process (liquid fraction = 1) are obtained at the time of 75 min, while cases of N = 5 and 7 have the same values at the time of 100 min (giving a slight advantage of N = 5). That is because the case of N = 3 has an inner tube with one curved corner that covers the bottom region and improves the heat transfer, expediting the melting process. The average Nu values show the heat transfer from the inner tube to the PCM. A significant drop happens at the beginning of the heating process due to the sharp reduction in the temperature difference between the surface of the inner tube and PCM. That keeps dropping steadily due to the melting process, in which some regions maintain the same temperature during the melting while the melted PCM (liquid phase) gets a higher temperature. Once all PCM gets melted, the temperature difference between PCM and the inner tube surface is almost zero, so the temperature and liquid fraction values are flattened. During the melting process, the total enthalpy values are higher for the trefoil case due to the high-temperature difference and the associated particle bond separation, while after the melting process, the thermal entropy almost diminished, and the liquid phase flow friction takes place to generate some frictional entropy. Comparing the three cases proves that the trefoil case enhances the melting process by at least 25% compared to the others.

As illustrated in Figure 4, the qualitative results present a visual representation of the variations among the different configurations, allowing for an initial understanding of their performance. However, a more comprehensive and quantitative analysis can be derived from the temporal curves depicted in Figure 5. These time-dependent curves meticulously illustrate the progression of both the average temperature and the liquid fraction of the phase change material (PCM) as they evolve during the heating process, ultimately converging on equilibrium values.

Focusing on the N = 3 configuration, we observe that a peak temperature of 312 K is attained, along with a complete phase transition to the liquid state (liquid fraction = 1), within a span of just 75 min. In stark contrast, the configurations with N = 5 and N = 7 reach similar thermal states at the 100-min mark, with the N = 5 configuration demonstrating a slight performance edge over N = 7. The expedited melting process observed in the N = 3 case can be attributed to its innovative trefoil geometry design, which features a single,

effectively curved corner that enhances surface contact with the PCM and minimizes the PCM thickness at the bottom with reduced thermal resistance. This design significantly improves heat transfer to the lower regions of the PCM, subsequently facilitating a quicker melting process.

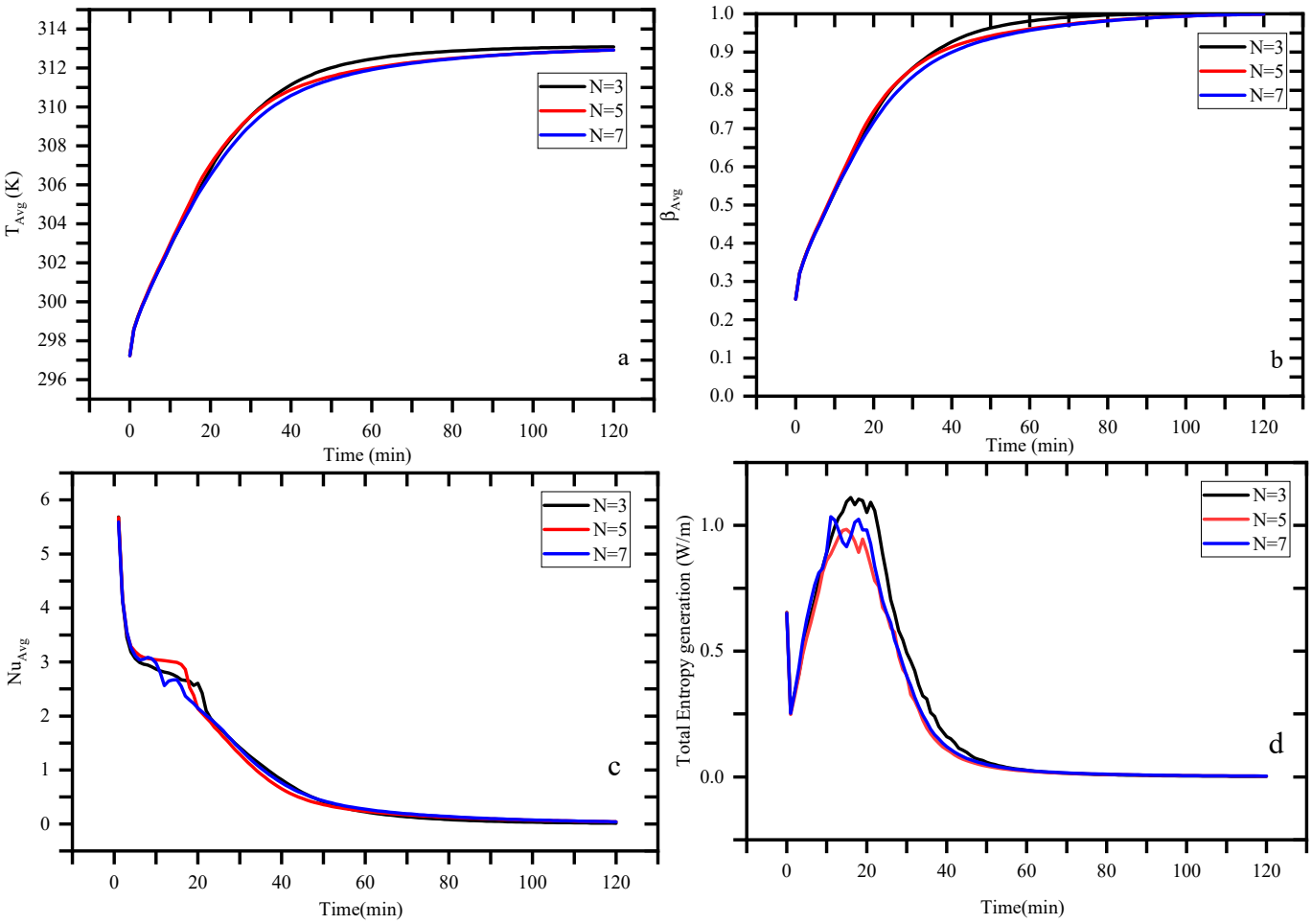

Figure 5. Influence of wave number on (**a**) average temperature, (**b**) average liquid fraction, (**c**) average Nusselt number, and (**d**) total entropy generation.

To quantitatively assess the heat transfer capabilities from the inner tube to the PCM, it is worth considering the average Nu values. Initially, an observable and significant drop in Nu is noted, a phenomenon occurring due to the rapid decrease in the temperature gradient between the surface of the inner tube and the PCM. As the melting process advances, the Nusselt number continues to decline steadily over time. This reduction is influenced by the complex dynamics inherent in the phase change process: certain segments of the PCM maintain a constant temperature while undergoing melting, whereas the regions that have transitioned to the liquid phase actively absorb heat, subsequently raising their temperatures. As the heating continues and once the PCM achieves total melting, the temperature differential between the PCM and the inner tube surface diminishes to near-zero levels, resulting in the flattening of both temperature and liquid fraction curves.

Throughout the melting phase, total enthalpy values remain highest in the configuration featuring the trefoil geometry (N = 3). This is primarily a result of the pronounced temperature difference across the PCM and the associated disruption of particle bonds as the material shifts to a liquid state. Following the complete phase transition, we observe a marked decrease in thermal entropy, while frictional entropy stemming from the flow of the liquid phase becomes increasingly significant in contributing to overall system dynamics.

Upon conducting a quantitative comparison of the three configurations, it becomes evident that the trefoil geometry (N = 3) yields at least a 25% improvement in the melting process relative to both the N = 5 and N = 7 designs. This substantial efficiency enhancement underscores the superiority of the trefoil design in optimizing heat transfer processes and accelerating phase change phenomena, ultimately highlighting its potential applications in thermal energy storage systems.

4.2. Effect of the External Tube Shape

The previous figures show that the inner tube shape may greatly improve the melting process by over 25%. Therefore, the impact of the external tube shape is also studied by keeping the inner tube in a circle shape, as shown in Figure 6.

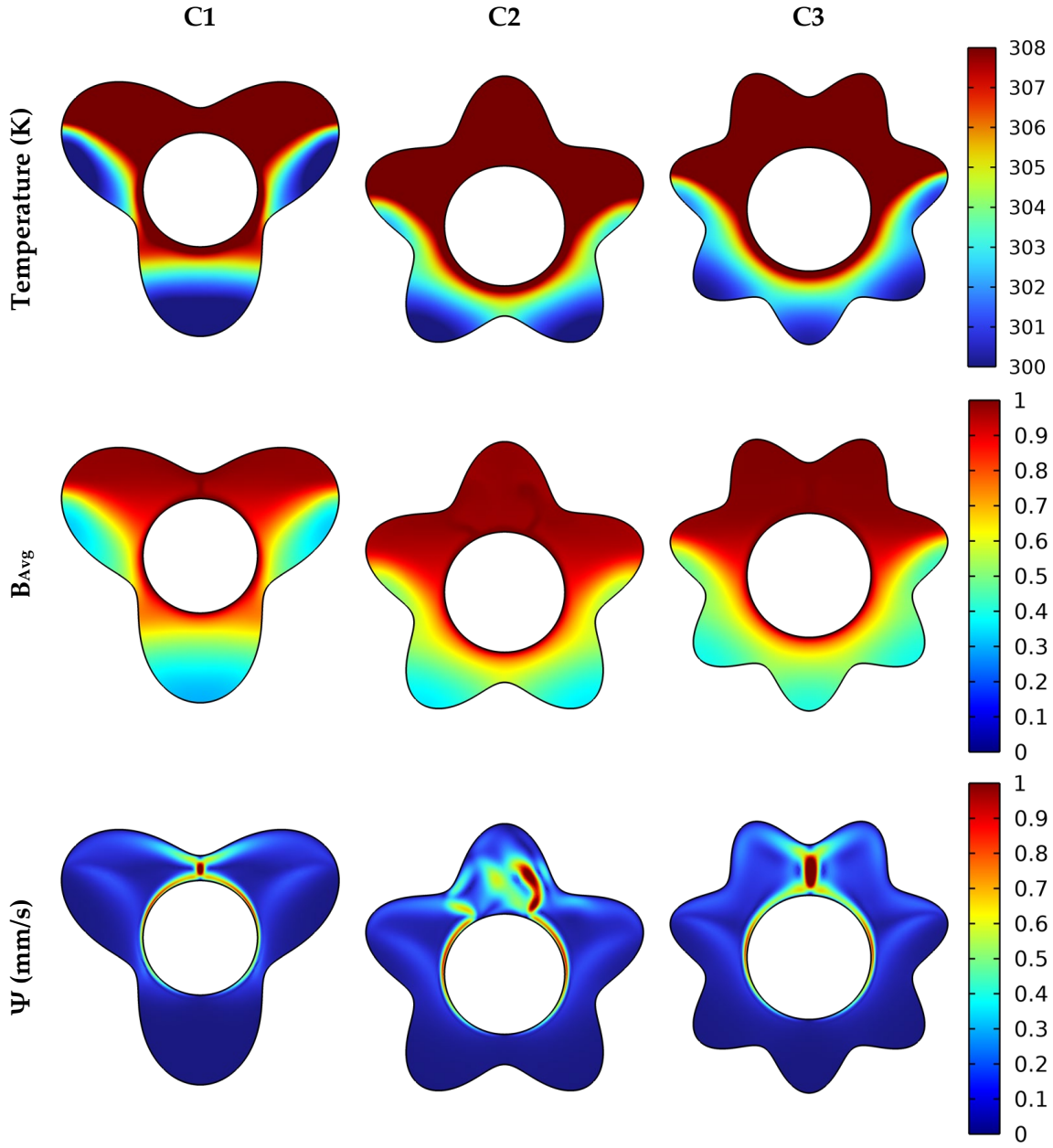

Figure 6. Effect of outer tube wave number on temperature, average liquid fraction, and velocity in t = 25 min.

A notable observation arises from the investigation of the influence of wave configurations on the external tube. Interestingly, the effect of varying the number of waves in the external tube exhibits a behavior that is contrary to that noted for the inner tube. Specifically, an increase in the number of waves within the external tube appears to restrict the flow of the PCM predominantly to the lower region of the tube, which mirrors the behavior witnessed in the trefoil-shaped inner tube design. However, in the case of the configuration with N = 7 waves, the extended curved corners result in increased thermal resistance. This is primarily due to the thicker regions along the external tube's surface, which impede the rate of heat transfer by slowing the propagation of thermal energy. Despite this increased resistance, the N = 7 configuration is identified as the most effective in terms of thermal performance compared to other external tube designs.

The examination of temperature distributions and melting process contours reveals that free convection plays a significant role in the upper sections of all external tube configurations. This phenomenon is predominantly driven by the buoyancy effect, wherein warmer fluid rises due to lower density, thereby enhancing circulation patterns and facilitating more efficient heat transfer. Furthermore, it is observed that velocity values in the upper regions are markedly higher, where a minimal distance between the inner and external tubes exists. This can be attributed to the elevated temperatures of the flow, which promotes a robust circulation pattern, consequently accelerating the melting process within these critical areas.

Additionally, a comparative analysis of the wavy designs of both the external and inner tubes brings to light a significant discrepancy in their respective influences on heat transfer efficiency. The inner tube is shown to exert a much more profound effect on the heat transfer process due to its function as the primary heating source within the system. This design increases the surface area available for heat transmission, thereby intensifying the overall heat transfer rate. Conversely, the external tube acts primarily as a heat sink, with its geometric configuration mainly determining the redistribution of the PCM rather than directly impacting the rate at which heat is delivered to the material.

These comprehensive findings emphasize that although the design of the external tube does exert a measurable influence on the system's thermal performance, it is ultimately the geometry of the inner tube that emerges as the critical determinant in optimizing heat transfer efficiency and enhancing the melting process of phase change materials. This insight prompts further investigation into the optimal design parameters for both tube configurations to maximize overall system effectiveness.

Figure 7 shows the quantitative results for the average temperature, average melting fraction, average Nusselt number, and total entropy generation. It is shown that the storage unit temperature approaches the heating source temperature after 135 min for cases N = 5 and 7, at which the PCM liquid fills the storage unit. For N = 3 cases, the time of 200 min is still insufficient to melt PCM fully. More than 45% of the melting process is enhanced for N = 5 and 7 compared to the case of N = 3.

To compare these values with the impact of the inner tube, the inner tube with N = 3 can melt all PCM within only half time (70 min). The enhancement of the use of the waved surface for the inner tube compared to that of the external one is 92.7% for the case of N = 3. Therefore, the waved inner tube is more important than the external one, especially when the inner tube is the heating surface. Keeping the external tube circular is better for reducing the thick regions and the thermal resistance. Then, Figure 7 emphasizes that there is no need for any wavy walls for the external tubes. Also, as explained before, the Nusselt number values show a drop trend due to the reduction in temperature difference between the heating surface and the PCM and external wall. The significant melting time is 25–100 min, which shows the units of N = 5 and 7 are better than that of the N = 3 case (which takes longer to have lower Nu values) due to better heat transfer and better heating of the PCM. Thus, the entropy generation values are higher at this time for N = 7, followed by N = 5 case as the melting process participates significantly in the thermal entropy

generation. After t = 100 min, the participation of entropy generation comes primarily from the PCM liquid flow friction.

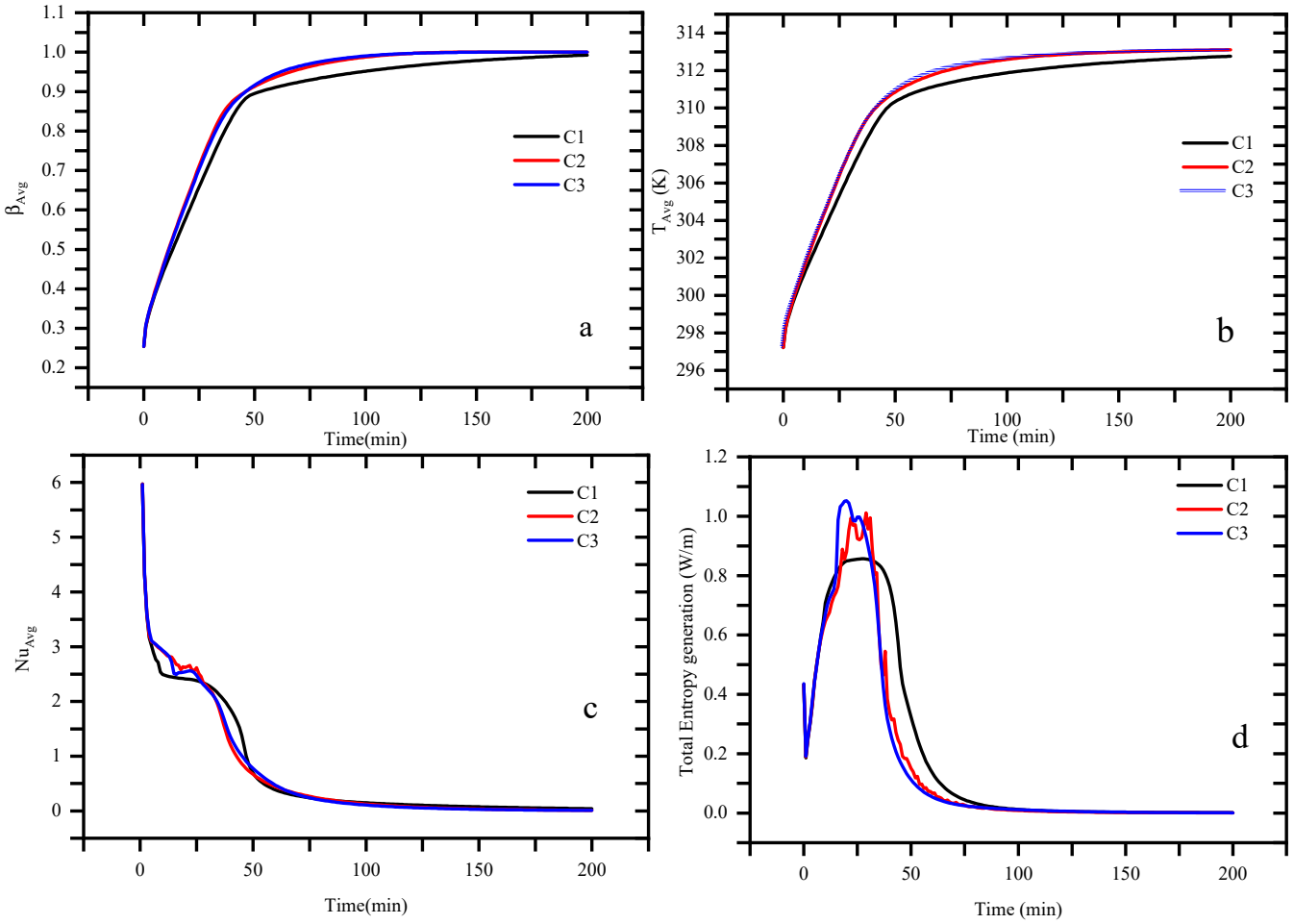

Figure 7. Effect of outer tube wave number on (**a**) average liquid fraction, (**b**) average temperature, (**c**) average Nusselt number, and (**d**) total entropy generation.

4.3. Effect of Nanoparticle Concentration

Adding nanoparticles to PCM proves its efficacy in reducing the thermal resistance (by improving the effective thermal conductivity), thus expediting the melting process. The concentration of copper nanoparticles is investigated for 0, 3, and 8 vol%. It is important to mention that adding more nanoparticles reduces the amount of PCM and then reduces the thermal energy stored. Thus, this study considers only up to 8% of nanoparticles. Also, as this study focuses on melting process enhancement, thermal conductivity is the main thermal property highlighted.

Figure 8 illustrates the temperature and melting contours of different cases, revealing that while the temperature profiles show only slight variations, the velocity contours demonstrate significant differences. Specifically, as the concentration of nanoparticles in the NePCM is increased, there is a corresponding rise in the effective density of the material. This increase in density is associated with a noticeable decrease in the velocity of the fluid, impacting the heat transfer dynamics. However, it is important to note that the contours themselves do not give a comprehensive picture of the enhancement of the melting process. For a more accurate assessment, the temporal profiles presented in Figure 9 are crucial as they provide deeper insights into the percentage of enhancement achieved through varying nanoparticle concentrations.

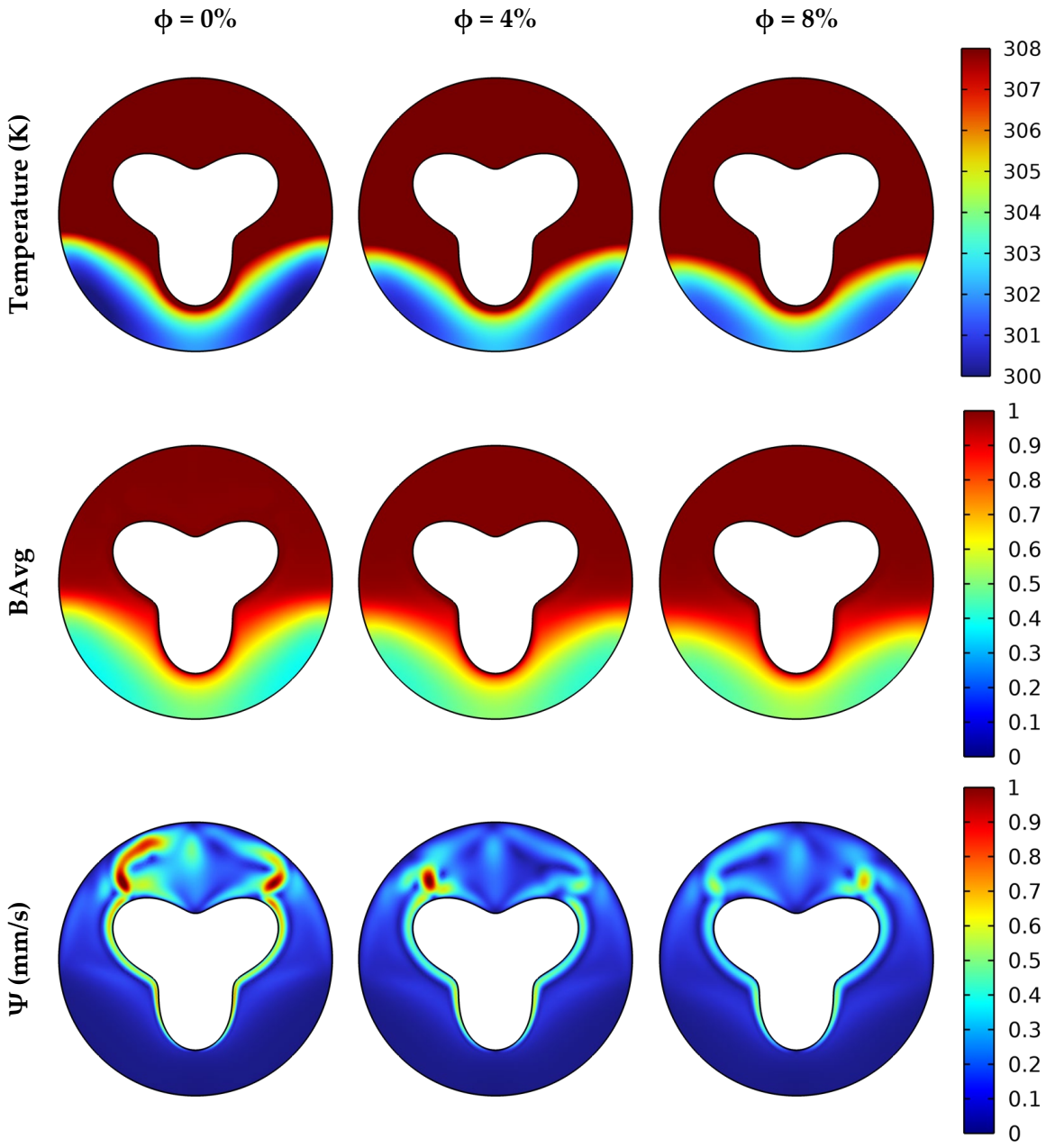

Figure 8. Effect of copper nanoparticle concentration on temperature, average liquid fraction, and velocity in t = 25 min.

The temporal analysis reveals that while pure PCM takes a total of 75 min to reach complete melting, the introduction of an 8 vol% nanoparticle concentration effectively reduces the melting duration to just 60 min. This results in an impressive improvement of approximately 20%. The underlying cause of this improvement lies in the enhanced thermal conductivity of the NePCM, which allows it to absorb heat much more rapidly. Consequently, the temperature of the PCM rises more effectively, leading to a decrease in the temperature difference between the inner wall and the NePCM, thus optimizing the heat transfer process.

Further insights can be gathered from the Nu values associated with the 8 vol% concentration case. These values underscore a significant improvement in heat transfer performance. The lowest Nu values are registered during this scenario, indicating a more efficient heat transfer process that elevates the PCM's temperature more swiftly compared to the other experimental cases examined.

The entropy generation profiles provide additional valuable information regarding the melting dynamics. In the initial 30 min, which encompasses the majority of the melting phase, the 8 vol% concentration demonstrates a marked increase in entropy generation. This increase is largely a consequence of the phase change process, wherein the absorption of thermal energy disrupts the solid particle bonds, thereby facilitating the transition from solid to liquid.

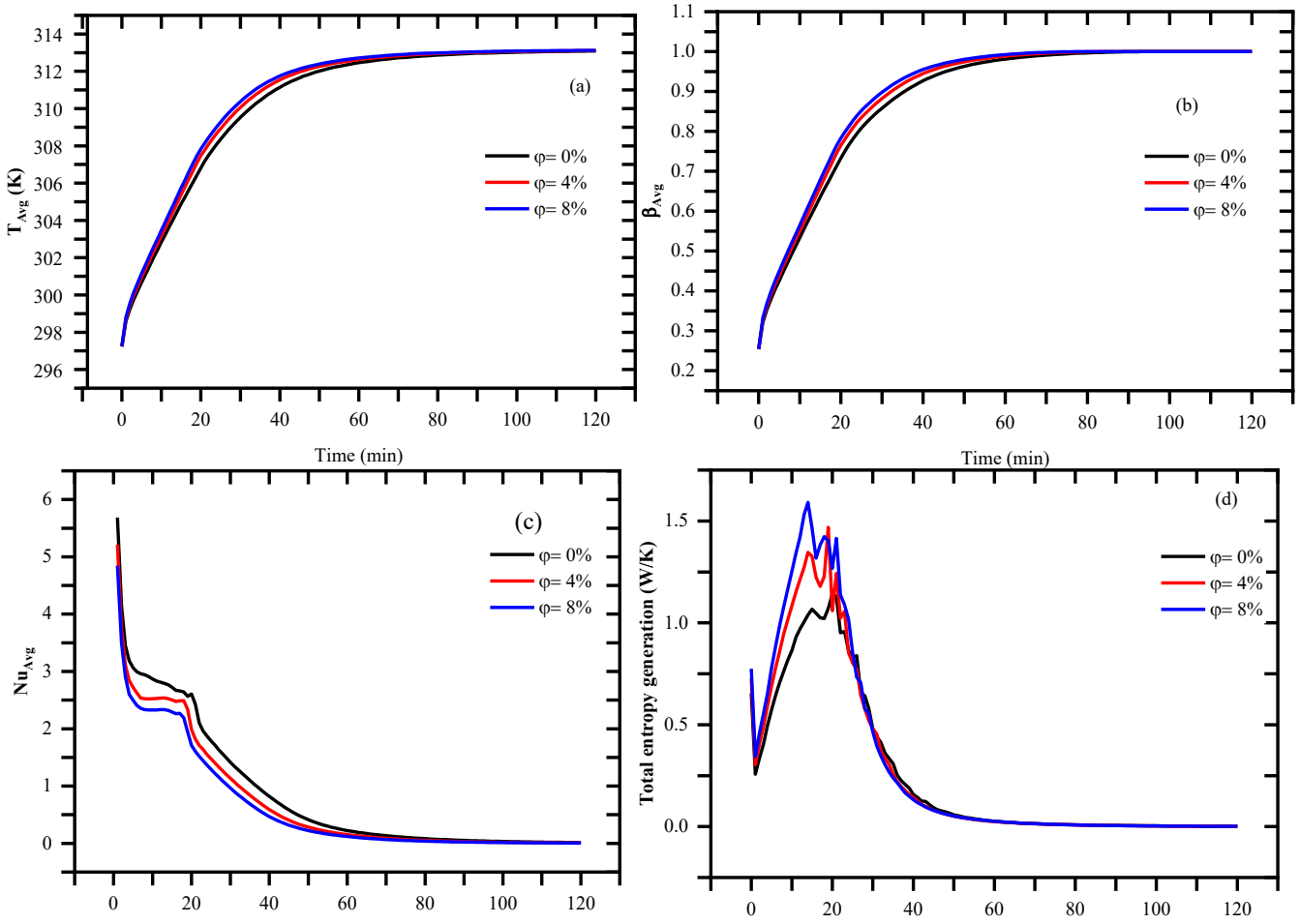

Figure 9. History of copper nanoparticle concentration influence on (**a**) average temperature, (**b**) average liquid fraction, (**c**) average Nusselt number, and (**d**) total entropy generation.

Once 30 min have elapsed, and as the melting process nears completion, a noticeable reduction in the temperature difference between the liquid PCM and the inner wall occurs. This diminishing temperature gradient results in a slowdown of the heat transfer rate and a subsequent decrease in thermal entropy generation. After this time threshold ($t > 30$ min), the contributions to entropy are predominantly due to the friction associated with the flow of liquid PCM, which remains relatively minor when compared to the thermal entropy generated during the phase change.

In summary, the entropy profiles strongly support the assertion that the 8 vol% concentration not only significantly augments heat transfer efficiency but also promotes a more uniform and effective melting process, rendering it the most advantageous configuration among those studied. This detailed analysis illustrates the critical interplay among concentration, heat transfer dynamics, and entropy generation, highlighting the benefits of incorporating nanoparticles into PCM systems.

5. Conclusions

Enhancing thermal storage units is essential for improving the efficiency of thermal and energy systems. This study presents valuable insights into how modifying the geometries of the inner and outer tubes, along with the incorporation of copper nanoparticles, can significantly enhance heat transfer and accelerate the melting process in shell-and-tube thermal storage units. The analysis focused on various wavy inner tube configurations—specifically, 3 wavy numbers (trefoil shape), 5 (cinquefoil shape), and 7 (heptafoil shape). Additionally, n-octadecane paraffin phase change material (PCM) was enriched with copper nanoparticles at volumetric concentrations of 0%, 4%, and 8%. Simulations of the melting process and PCM flow dynamics were conducted using COMSOL Multiphysics, with the inner tube maintained at a temperature of 308 K and the external tube being adiabatic. The key findings reveal several important aspects:

1. The trefoil-shaped inner tube (N = 3) demonstrated remarkable results, reducing melting by over 25% compared to the cinquefoil and heptafoil shapes, with complete melting achieved in approximately 75 min.
2. The wavy geometry of the inner tube plays a crucial role in heat transfer and the melting process significantly, outperforming the effects of the external tube geometry by about 92.7%. A circular external tube was found to be highly effective compared to wavy surfaces in minimizing thermal resistance within the PCM.
3. The addition of 8 vol% copper nanoparticles to the PCM resulted in a substantial 20% reduction in melting time compared to pure PCM, thereby further improving the thermal performance of the system.

Given these findings, the study recommends the use of a trefoil inner tube (N = 3) combined with 8 vol% copper nanoparticles in PCM for optimal performance. The trefoil geometry not only enhances heat transfer through an increased surface area but also effectively accelerates the melting process by targeting the bottom region of the PCM with one of its corners. Advances in modern manufacturing techniques make the creation of such geometries both feasible and cost-effective.

Looking ahead, future research can broaden the scope by evaluating alternative PCMs with higher melting points to widen the range of applications. Additionally, a comprehensive economic analysis for both geometries and nanoparticle additions would be beneficial to assess the feasibility and scalability of these innovative designs within practical energy systems.

Author Contributions: Conceptualization, O.Y.; Methodology, O.Y.; Software, N.A.A.Q. and A.A.; Validation, N.A.A.Q. and A.A.; Formal analysis, O.Y., N.A.A.Q., A.A. and A.B.; Investigation, A.A. and A.B.; Resources, O.Y. and A.A.; Data curation, A.A. and A.B.; Writing—original draft, O.Y., N.A.A.Q., A.A. and A.B.; Writing—review & editing, O.Y., N.A.A.Q., A.A. and A.B.; Visualization, A.B.; Supervision, O.Y.; Project administration, A.A.; Funding acquisition, O.Y. All authors have read and agreed to the published version of the manuscript.

Funding: This research was funded by the Prince Sattam bin Abdulaziz University project number (PSAU/2024/01/29335).

Data Availability Statement: Dataset available on request from the authors.

Acknowledgments: The authors extend their appreciation to Prince Sattam bin Abdulaziz University for funding this research work through the project number (PSAU/2024/01/29335).

Conflicts of Interest: The authors declare no conflict of interest.

References

1. Kant, K.; Anand, A.; Shukla, A.; Sharma, A. Heat transfer study of building integrated photovoltaic (BIPV) with nano-enhanced phase change materials. *J. Energy Storage* **2020**, *30*, 101563. [CrossRef]
2. Kant, K.; Shukla, A.; Sharma, A.; Biwole, P.H. Heat transfer studies of photovoltaic panel coupled with phase change material. *Solar Energy* **2016**, *140*, 151–161. [CrossRef]

3. Nithyanandam, K.; Stekli, J.; Pitchumani, R. High-temperature latent heat storage for concentrating solar thermal (CST) systems. In *Advances in Concentrating Solar Thermal Research and Technology*; Elsevier: Amsterdam, The Netherlands, 2017; pp. 213–246. [CrossRef]
4. Guo, H.; Jiao, W.; Jin, H.; Yuan, Z.; He, X. Microsphere Structure Composite Phase Change Material with Anti-Leakage, Self-Sensing, and Photothermal Conversion Properties for Thermal Energy Harvesting and Multi-Functional Sensor. *Adv. Funct. Mater.* **2023**, *33*, 2209345. [CrossRef]
5. Zhang, Y.; Wu, K.; Fu, Q. A Structured Phase Change Material with Controllable Thermoconductive Highways Enables Unparalleled Electricity via Solar-Thermal-Electric Conversion. *Adv. Funct. Mater.* **2022**, *32*, 2109255. [CrossRef]
6. Hu, Z.; Jiang, S.; Sun, Z.; Li, J. Numerical simulation of fin arrangements on the melting process of PCM in a rectangular unit. *Renew. Energy* **2024**, *220*, 119677. [CrossRef]
7. Fahad, M.K.; Subah, S.; Ifraj, N.F.; Tahsin, S.H.; Alvi, T.R.; Hasan, M.J. Comparative analysis on melting performance of PCM using rectangular and branching fin configurations in a shell and tube type thermal energy storing unit. *J. Energy Storage* **2024**, *91*, 112048. [CrossRef]
8. Liu, H.-Y.; Qu, B.-C.; Wu, C.-M.; Li, Y.-R. Numerical study of PCM melting performance in a rectangular container with various longitudinal fin structures. *J. Energy Storage* **2024**, *94*, 112529. [CrossRef]
9. Jiang, J.; Shao, G.; Cui, H.; Zhu, H.; Li, H. Numerical study on the melting performance of PCM by fractal fins in three-tube heat storage system. *Numer. Heat. Transf. A Appl.* **2024**, 1–19. [CrossRef]
10. Rokhforouz, M.; Sheikholeslami, M. Numerical investigation of the process of melting and solidification within a parabolic trough solar collector using nanoparticles and fins. *J. Clean. Prod.* **2024**, *434*, 140269. [CrossRef]
11. Waqas, H.; Hasan, M.J.; Naqvi, S.M.R.S.; Liu, D.; Muhammad, T.; Eldin, S.M.; Kang, C. Enhancing the performance of thermal energy storage by adding nanoparticles with paraffin phase change materials. *Nanotechnol. Rev.* **2024**, *13*, 20230180. [CrossRef]
12. Briache, A.; Afass, A.; Ouardouz, M.; Ahachad, M.; Mahdaoui, M. A Comparative Analysis of Enhancement Techniques in a PCM-Embedded Heat Sink: Fin forms, Nanoparticles, and Metal Foam. *Int. J. Heat. Mass Transf.* **2024**, *229*, 125730. [CrossRef]
13. Chaurasiya, S.K.; Singh, S. High power and energy density of a wavy PCM unit embedded in a solar air heater utilizing fractional porous media. *Appl. Therm. Eng.* **2024**, *236*, 121843. [CrossRef]
14. Liu, J.; Xiao, Y.; Nie, C. Pore-scale study of melting characteristic of phase change material embedded with novel open-celled metal foam. *Int. J. Heat. Mass Transf.* **2024**, *228*, 125634. [CrossRef]
15. Zhang, S.; Zhu, Y.; Zhang, H.; Xu, F.; Sun, L.; Xia, Y.; Lin, X.; Peng, H.; Ma, L.; Li, B.; et al. Cadmium Sulfide—Reinforced Double-Shell Microencapsulated Phase Change Materials for Advanced Thermal Energy Storage. *Polymers* **2022**, *15*, 106. [CrossRef] [PubMed]
16. Ben Khedher, N.; Bantan, R.A.; Kolsi, L.; Omri, M. Performance investigation of a vertically configured LHTES via the combination of nano-enhanced PCM and fins: Experimental and numerical approaches. *Int. Commun. Heat Mass Transf.* **2022**, *137*. [CrossRef]
17. Mourad, A.; Abderrahmane, A.; Abed, A.M.; Toghraie, D.; Ahmed, S.E.; Guedri, K.; Fazilati, M.A.; Marzouki, R.; Younis, O. Numerical investigation of a snowflake-shaped fin-assisted latent heat storage system using nanofluid. *J. Energy Storage* **2022**, *55*, 105775. [CrossRef]
18. Qasem, N.A.; Abderrahmane, A.; Belazreg, A.; Younis, O.; Khetib, Y.; Guedri, K. Investigation of phase change heat transfer in a rectangular case as function of fin placement for solar applications. *Case Stud. Therm. Eng.* **2024**, *54*, 103996. [CrossRef]
19. Peng, Q.; Duan, W.; Sun, X.; Jiang, F.; Luo, Y.; Zhai, J. Evaluation of the melting process of phase change materials in a tilted rectangular container: Experimental study. *Energy Built Environ.* 2024, *in press*. [CrossRef]
20. Khalaf, A.F.; Rashid, F.L.; Letif, S.A.; Ameen, A.; Mohammed, H.I. A Numerical Study of the Effect of Water Speed on the Melting Process of Phase Change Materials Inside a Vertical Cylindrical Container. *Appl. Sci.* **2024**, *14*, 3212. [CrossRef]
21. Sultan, H.S.; Mohammed, H.I.; Biswas, N.; Togun, H.; Ibrahem, R.K.; Mahdi, J.M.; Yaïci, W.; Keshmiri, A.; Talebizadehsardari, P. Revolutionizing the latent heat storage: Boosting discharge performance with innovative undulated phase change material containers in a vertical shell-and-tube system. *J. Comput. Des. Eng.* **2024**, *11*, 122–145. [CrossRef]
22. Aziz, S.; Amin, N.A.M.; Majid, M.S.A.; Belusko, M.; Bruno, F. CFD simulation of a TES tank comprising a PCM encapsulated in sphere with heat transfer enhancement. *Appl. Therm. Eng.* **2018**, *143*, 1085–1092. [CrossRef]
23. Chan, C.W.; Tan, F.L. Solidification inside a sphere—An experimental study. *Int. Commun. Heat Mass Transf.* **2006**, *33*, 335–341. [CrossRef]
24. Ehms, J.H.N.; De Césaro Oliveski, R.; Rocha, L.A.O.; Biserni, C. Theoretical and numerical analysis on phase change materials (PCM): A case study of the solidification process of erythritol in spheres. *Int. J. Heat Mass Transf.* **2018**, *119*, 523–532. [CrossRef]
25. Qin, Z.; Ji, C.; Low, Z.H.; Tong, W.; Wu, C.; Duan, F. Geometry effect of phase change material container on waste heat recovery enhancement. *Appl. Energy* **2022**, *327*, 120108. [CrossRef]
26. Huang, B.; Yang, S.; Wang, J.; Lund, D. Optimizing the shape of PCM container to enhance the melting process. *Oxf. Open Energy* **2022**, *1*, oiab006. [CrossRef]
27. Boujelbene, M.; Mohammed, H.I.; Majdi, H.S.; Babaei-Mahani, R.; Talebizadehsardari; Rahbari, A. Melting performance of nano-enhanced phase change materials in a triple-tube heat exchanger with zigzag-shaped tubes. *J. Energy Storage* **2023**, *67*, 107484. [CrossRef]

28. Li, Z.; Sheikholeslami, M.; Shafee, A.; Haq, R.; Khan, I.; Tlili, I.; Kandasamy, R. Solidification process through a solar energy storage enclosure using various sizes of Al_2O_3 nanoparticles. *J. Mol. Liq.* **2019**, *275*, 941–954. [CrossRef]
29. Najafpour, N.; Adibi, O. Melting enhancement of latent heat thermal energy storage by implementing new geometric design. *Appl. Therm. Eng.* **2024**, *239*, 122066. [CrossRef]
30. NematpourKeshteli, A.; Iasiello, M.; Langella, G.; Bianco, N. Thermal enhancement techniques for a lobed-double pipe PCM thermal storage system. *Appl. Therm. Eng.* **2023**, *233*, 121139. [CrossRef]
31. Qaiser, R.; Khan, M.M.; Khan, L.A.; Irfan, M. Melting performance enhancement of PCM based thermal energy storage system using multiple tubes and modified shell designs. *J. Energy Storage* **2021**, *33*, 102161. [CrossRef]
32. Khedher, N.B.; Biswas, N.; Togun, H.; Mohammed, H.I.; Mahdi, J.M.; Ibrahem, R.K.; Talebizadehsardari, P. Geometry modification of a vertical shell-and-tube latent heat thermal energy storage system using a framed structure with different undulated shapes for the phase change material container during the melting process. *J. Energy Storage* **2023**, *72*, 108365. [CrossRef]
33. Darzi, A.A.R.; Jourabian, M.; Farhadi, M. Melting and solidification of PCM enhanced by radial conductive fins and nanoparticles in cylindrical annulus. *Energy Convers Manag.* **2016**, *118*, 253–263. [CrossRef]
34. Szczyglewska, P.; Feliczak-Guzik, A.; Nowak, I. Nanotechnology–General Aspects: A Chemical Reduction Approach to the Synthesis of Nanoparticles. *Molecules* **2023**, *28*, 4932. [CrossRef] [PubMed]
35. Álvarez-Chimal, R.; Arenas-Alatorre, J.Á. Green synthesis of nanoparticles. A biological approach. In *Advances in Green Chemistry [Working Title]*; IntechOpen: London, UK, 2023. [CrossRef]
36. Nowack, B. The behavior and effects of nanoparticles in the environment. *Environ. Pollut.* **2009**, *157*, 1063–1064. [CrossRef] [PubMed]
37. Shanmugam, S. Nanotechnology. 2019. Available online: https://books.google.com/books?hl=fr&lr=&id=cNWcDwAAQBAJ&oi=fnd&pg=PA1&ots=w-hwUYsaUk&sig=kUUhIShMfc6txiTjsHykZcl965o (accessed on 21 June 2024).
38. Faraji, H.; El Alami, M.; Arshad, A.; Faraji, M. Numerical simulation of the melting of a NePCM for cooling of electronic components. *Therm. Sci. Eng. Prog.* **2021**, *21*, 100766. [CrossRef]
39. Hasnain, F.U.; Irfan, M.; Khan, M.M.; Khan, L.A.; Ahmed, H.F. Melting performance enhancement of a phase change material using branched fins and nanoparticles for energy storage applications. *J. Energy Storage* **2021**, *38*, 102513. [CrossRef]
40. Al-Jethelah, M.S.M.; Tasnim, S.H.; Mahmud, S.; Dutta, A. Melting of nano-phase change material inside a porous enclosure. *Int J. Heat. Mass Transf.* **2016**, *102*, 773–787. [CrossRef]
41. Ebrahimi, A.; Dadvand, A. Simulation of melting of a nano-enhanced phase change material (NePCM) in a square cavity with two heat source–sink pairs. *Alex. Eng. J.* **2015**, *54*, 1003–1017. [CrossRef]
42. Kalbande, V.; Fating, G.; Mohan, M.; Rambhad, K.; Sinha, A.K. Experimental and theoretical study for suitability of hybrid nano enhanced phase change material for thermal energy storage applications. *J. Energy Storage* **2022**, *51*, 104431. [CrossRef]
43. Sheikholeslami, M.; Khalili, Z.; Scardi; Ataollahi, N. Concentrated solar photovoltaic cell equipped with thermoelectric layer in presence of nanofluid flow within porous heat sink: Impact of dust accumulation. *Sustain. Cities Soc.* **2023**, *98*, 104866. [CrossRef]
44. Tuli, S.S.; Saha, L.K.; Roy, N.C. Effect of inclined magnetic field on natural convection and entropy generation of non-Newtonian ferrofluid in a square cavity having a heated wavy cylinder. *J. Eng. Math.* **2023**, *141*, 6. [CrossRef]
45. Darzi, A.R.; Afrouzi, H.H.; Khaki, M.; Abbasi, M. Unconstrained melting and solidification inside rectangular enclosure. *J. Fundam. Appl. Sci.* **2015**, *7*, 436. [CrossRef]
46. Voller, V.R.; Prakash, C. A fixed grid numerical modelling methodology for convection-diffusion mushy region phase-change problems. *Int. J. Heat Mass Transf.* **1987**, *30*, 1709–1719. [CrossRef]
47. Mat, S.; Al-Abidi, A.A.; Sopian, K.; Sulaiman, M.Y.; Mohammad, A.T. Enhance heat transfer for PCM melting in triplex tube with internal–external fins. *Energy Convers. Manag.* **2013**, *74*, 223–236. [CrossRef]
48. Hosseinizadeh, S.F.; Darzi, A.A.R.; Tan, F.L. Numerical investigations of unconstrained melting of nano-enhanced phase change material (NEPCM) inside a spherical container. *Int. J. Therm. Sci.* **2012**, *51*, 77–83. [CrossRef]
49. Kalaiselvam, S.; Parameshwaran, R.; Harikrishnan, S. Analytical and experimental investigations of nanoparticles embedded phase change materials for cooling application in modern buildings. *Renew. Energy* **2012**, *39*, 375–387. [CrossRef]
50. Brinkman, H.C. The Viscosity of Concentrated Suspensions and Solutions. *J. Chem. Phys.* **1952**, *20*, 571. [CrossRef]
51. Maxwell, J. A Treatise on Electricity and Magnetism—Google Scholar. Available online: https://scholar.google.com/scholar?hl=fr&as_sdt=0,5&q=J.+Maxwell,+A+Treatise+on+Electricity+and+Magnetism,+Oxford+University+Press,+Cambridge,+UK,+1904.&btnG= (accessed on 20 July 2024).
52. Heat and Mass Transfer in Packed Beds—Noriaki Wakao, Seiichirō Kagei—Google Livres. Available online: https://books.google.dz/books?hl=fr&lr=&id=Ya5hzOgC05wC&oi=fnd&pg=PR9&ots=74wWZW3xEY&sig=T9nkNx7WEJyunlPBmuXwShqp_n0&redir_esc=y#v=onepage&q&f=false (accessed on 21 June 2024).
53. Khodadadi, J.M.; Zhang, Y. Effects of buoyancy-driven convection on melting within spherical containers. *Int. J. Heat Mass Transf.* **2001**, *44*, 1605–1618. [CrossRef]
54. Esapour, M.; Hosseini, M.J.; Ranjbar, A.A.; Pahamli, Y.; Bahrampoury, R. Phase change in multi-tube heat exchangers. *Renew. Energy* **2016**, *85*, 1017–1025. [CrossRef]

55. Ye, W.-B.; Zhu, D.-S.; Wang, N. Numerical simulation on phase-change thermal storage/release in a plate-fin unit. *Appl. Therm. Eng.* **2011**, *31*, 3871–3884. [CrossRef]
56. Mahdi, J.M.; Nsofor, E.C. Melting enhancement in triplex-tube latent thermal energy storage system using nanoparticles-fins combination. *Int. J. Heat Mass Transf.* **2017**, *109*, 417–427. [CrossRef]